Counter-Gravity Casting of Al Alloys: Microstructure and Properties

K. Georgarakis, J. Vian, D. Sgardelis, B. Souchon, Y. Chao, K. Konakoglou, M. Stiehler, and M. Jolly

Abstract

Counter-gravity casting can improve the structural integrity of castings by eliminating defects resulting from the turbulent flow of the molten metal during filling. The Constrained Rapid Induction Melting Single Shot Up-casting (CRIMSON) is an alternative counter-gravity casting approach designed for improving energy efficiency in castings in line with the concept of sustainable foundry. In this work, the microstructure and properties of the hypoeutectic 354 Al alloy produced by CRIMSON counter-gravity casting is investigated and compared with specimens produced by conventional gravity sand casting in the as-cast condition. The results indicate significant reduction in porosity, oxide inclusions and bifilms for the CRIMSON counter-gravity cast samples compared to that in conventional gravity cast samples in line with the controlled liquid flow of the counter-gravity filling. This can lead to significant improvements in terms of the casting yield, the expected fatigue resistance of the alloys as well as efficiency of the casting processes in terms of energy, materials use and greenhouse emissions. Furthermore, similar dendritic microstructure consisting of α-Al dendrites, Al–Si eutectic and intermetallic compounds in small volume fraction was observed for both CRIMSON and gravity cast samples. The mechanical behaviour was also evaluated using tensile tests and hardness tests.

Keywords

CRIMSON casting • Al alloys • Mechanical properties

Introduction

Metal casting is by nature an energy-intensive process as it typically involves the heating up and melting of metals and alloys at elevated temperatures. Most often the energy consumption, however, is much higher than what is thermodynamically necessary, which can be largely attributed to the low efficiency of conventional casting processes and foundry procedures. Furthermore, castings often suffer from various types of defects as a result of phenomena including shrinkage during solidification, entrainement, misruns, hot tears, and residual stresses [1, 2]. It is estimated that about 80% of the casting implications could be attributed to the entrained defects, mainly caused during filling. Non-controlled filling velocity, such as usually employed in gravity casting, can cause turbulence in the liquid flow resulting in defects such as oxide bifilms and air entrainment, that significantly deteriorate the structural integrity and engineering performance of castings [3–5]. To limit these defects, a maximum filling velocity criterion has been suggested by Campbell [6]; for Al alloys this equals to 0.5 ms^{-1}. Counter-gravity casting processes can actually provide such control in metal flow during filling improving the quality and structural integrity of castings [6, 7]. To this effect, the constrained rapid induction melting single shot up-casting (CRIMSON) has been designed to offer energy savings, increased casting yield, and reduce the propensity of casting defects such as double oxide films (DOF) and porosity [8]. CRIMSON concept suggests the use of high-quality raw materials and uses an induction furnace to rapidly melt the appropriate quantity of metal for filling a single mould thus making the traditional holding step redundant. Then the liquid is transferred to a computer-controlled casting unit that delivers the melt into the mould using counter-gravity filling. The mould including the running and feeding systems, as well as the liquid metal flows can be optimized by using casting computational fluid dynamic calculations [9].

K. Georgarakis (✉) · J. Vian · D. Sgardelis · B. Souchon · Y. Chao · K. Konakoglou · M. Stiehler · M. Jolly
School of Aerospace, Transport and Manufacturing, Cranfield University, Cranfield, UK
e-mail: k.georgarakis@cranfield.ac.uk

S. Broek (ed.), *Light Metals 2023*, The Minerals, Metals & Materials Series,
https://doi.org/10.1007/978-3-031-22532-1_144

Aluminum alloys are widely used as structural materials in numerous applications including in automotive and aerospace industries. Using appropriate alloy design such as addition of rare earth elements and appropriate manufacturing processes, aluminium alloys can reach mechanical (yield) strength as high as 1 GPa or higher [10–12]. More common industrial aluminium cast alloys however, can reach up to 320 MPa yield strength with appropriate processing. In particular, Al–Si–cast alloys show excellent castability, and are commonly used for the production of complex-shape parts with high specific strength due to their response to aging treatment [13, 14].

In this work, the hypoeutectic 354 Al alloy produced by CRIMSON counter-gravity casting and conventional gravity sand casting is investigated, in the as-cast condition, aiming to identify differences in the structural integrity and properties resulting from the difference in the casting process. In both processes, similar types of silica sand moulds were used in order to focus on the effect of the counter-gravity filling of CRIMSON casting.

Materials and Methods

The A354 Al alloy was used in this work. The raw material was in the form of direct chill (DC) billets, in a clean degassed condition from the metal supplier. Table 1 presents the chemical composition, typical for 354 Al alloy. Sand moulds were used to cast the alloy using (a) CRIMSON counter-gravity process and (b) conventional gravity casting for comparison. An assembly of six tensile bar specimens was produced with each casting as shown in Fig. 1. The tensile bar specimens had a gauge length of 75 mm and diameter of 12.5 mm, respectively, in line with the ASTM E8/E8M standards. A SIEMENS D5005 diffractometer using $Cu - K_{\alpha}$ radiation was employed to study the crystal structure of the cast specimens. Measurements were taken at various areas of the castings as shown in Fig. 2c. The samples (cross sections) were observed with a Leica (DM 2700 M RL/TL) optical microscope (OM) equipped with a CCD camera. A TESCAN LYRA3 scanning electron microscope (SEM) equipped with energy-dispersive spectroscopy (EDS) was employed for the investigation of the microstructure. The metallographic preparation included chemical etching with Keller's agent. Tensile tests were performed using an INSTRON 5500R instrument and a strain rate of 2.22×10^{-4} s^{-1}. At least 3 measurements were conducted per casting method sample. Hardness measurements were performed on the as-cast vertically cut disks from the tensile bars, using a 10 kg applied load for a holding time of 12 s. Hardness values presented in this work are the average value of at least 10 measurements.

Results and Discussion

Figure 2a, b show XRD patterns from five different areas of CRIMSON and gravity cast specimens, respectively. Figure 2c indicates the position of these five areas on a tensile bar specimen; positions 1 and 2 are on the top part of the sample, 3 in the middle (gauge section) and position 4 in the lower part—close to the runner. At positions 1–4, XRD spectra were taken at the cross section of the specimens. Position 5 is found in the middle part (gauge section) and

Table 1 Chemical composition of an A354 Al alloy

	Si (wt.%)	Mg (wt.%)	Cu (wt.%)	Fe (wt.%)	Mn (wt.%)	Ti (wt.%)	Al
A354	9	0.5	1.8	0.2	0.1	0.2	Balance

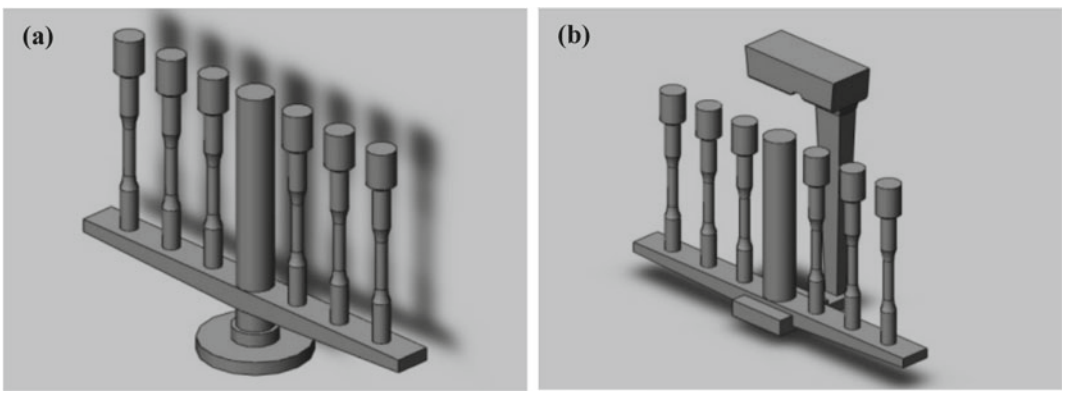

Fig. 1 Schematic illustrations of the mould designs; **a** CRIMSON casting and, **b** gravity casting [8]

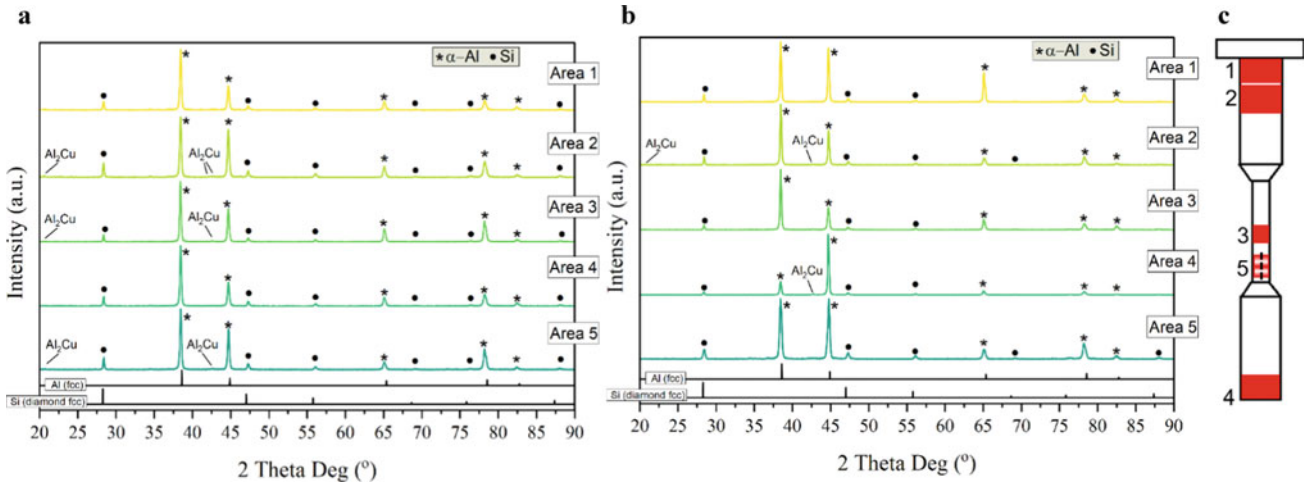

Fig. 2 XRD patterns of **a** the CRIMSON cast A354 alloy and, **b** the gravity-cast A354 alloy. **c** schematic illustration showing the five different areas/positions where XRD measurements were conducted. Areas 1–4 were cut across the solidification direction and area 5 vertical to the solidification direction

represents a longitudinal section, vertical to the solidification direction. As expected, the main reflections in the XRD spectra correspond to Al fcc and Si phases, whereas smaller reflections indicate the presence of θ-Al_2Cu phases in both CRIMSON and gravity-cast samples. These findings are typical for hypoeutectic aluminium–silicon–copper alloys. Comparing the XRD spectra for the two samples, no significant differences can be identified. The presence of other anticipated precipitated intermetallic phases, such as Q-$Al_5Cu_2Mg_8Si_6$, π-$Al_8FeMg_3Si_6$ and β-Al_5FeSi cannot be reliably identified with the XRD in this case due to their small volume fractions as well the overlapping of their reflections with those for Al and Si. However, evidence of such intermetallics were found during microscopical SEM analysis and will be discussed later on. A close observation of the pattern corresponding to position 4 of the gravity cast sample in Fig. 2b, one can notice a different intensity ratio between the (111) reflection at 37° $2-\theta$ angle and (200) reflection at 45° $2-\theta$ angle peak indicating a small increase of the (200) orientation compared to the other positions of the specimen. This must be related with a difference in the heat dissipation field during solidification of the gravity cast sample that is probably affected by the proximity of position 4 to the runner and the downsprue, Fig. 1b.

Optical micrographs taken from the centre and the mould-contacting edge of the cross-section at position 3 (Fig. 2c) of CRIMSON and gravity-cast samples are shown in Fig. 3. A clear difference in porosity can be observed. For the CRIMSON samples, Fig. 3a, b, some small pores mainly related to solidification shrinkage can be observed. On the other hand, for the gravity cast samples, Fig. 3c, d, in addition to the small pores related to shrinkage, pores significantly larger in size (up to 250 μm) with spherical and non-spherical shapes can be observed that may be resulting from air entrainment as well as oxide-induced defects [15, 16]. The microstructural features for both samples, Fig. 3, are typical for hypoeutectic Al–Si alloys with α-Al primary dendrites (light-coloured areas) surrounded by Al/Si eutectic phases (dark-coroured areas). The main microstructural features are comparable for both casting methods. Secondary dendrites arms spacing (SDAS) was found to be 31.8 ± 6.2 μm and 28.4 ± 4.7 μm for CRIMSON and gravity casting respectively.

Figure 4a shows an SEM micrograph from a gravity-cast A354 sample focusing on a pore wrapped up in an oxide that would possibly resemble a double oxide film (DOF). Figure 4b reveals the elemental content at various points of these defects numbered from 1 to 4. The high content of oxygen can be indicative of the presence of oxides such as Al_2O_3 supporting the hypothesis for the formation of double oxide films. DOF is a significant type of defect that is caused by surface turbulent flow during filling, which leads to the folding and breaking of the surface oxide film [15]. It is noted that these types of DOF defects have been mostly found in the gravity-cast samples suggesting that under the controlled liquid flow achieved by the counter-gravity filling of the CRIMSON casting can effectively reduce (or eliminate) the formation of double oxide films.

Figure 5 shows an SEM micrograph (accompanied by element maps) from a CRIMSON cast sample, depicting an area with Al dendrites, eutectic Al/Si colonies and intermetallic phases. The element mapping clearly indicates the distribution of Cu and Mg in different intermetallic phases. To further explore the formation of intermetallics in the cast alloys, Fig. 6 illustrates some intermetallic phases found in

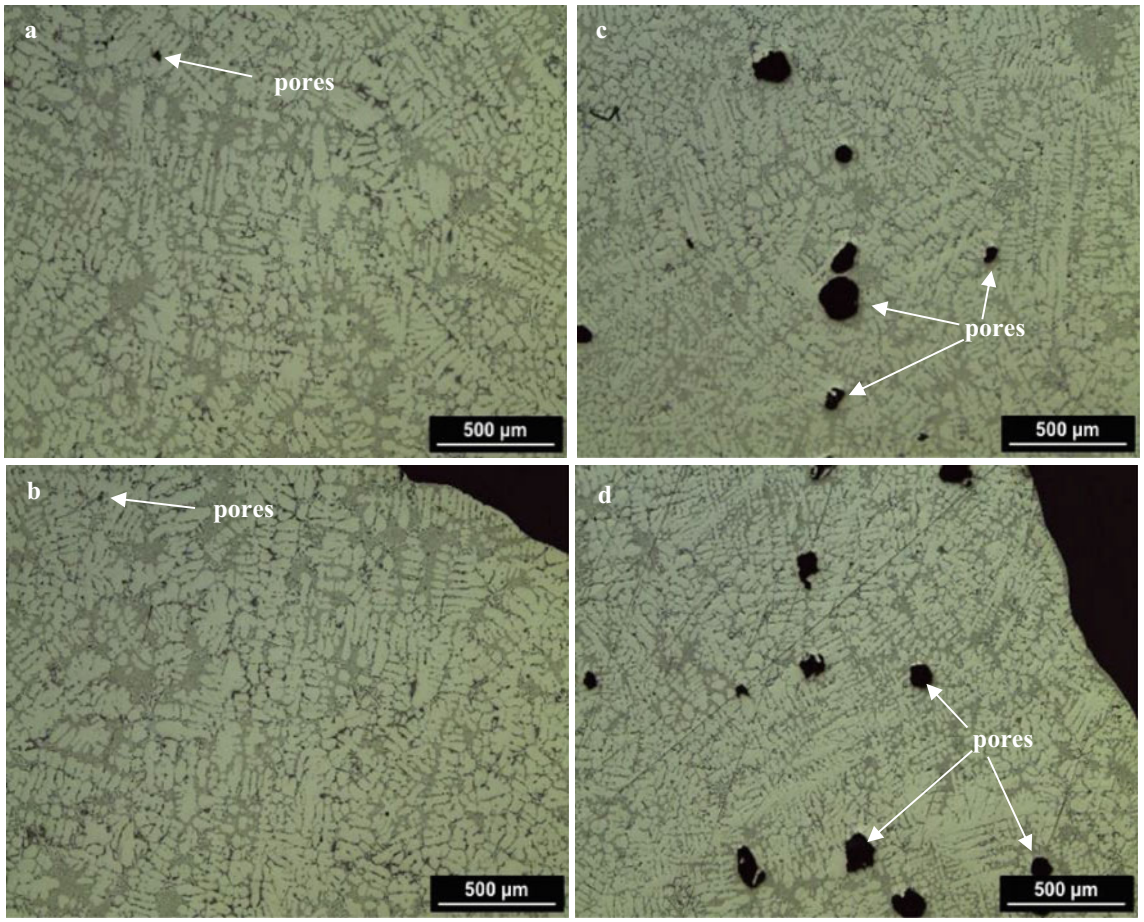

Fig. 3 Optical micrographs of the cross-section at the gage area (position 3): **a** CRIMSON casting at centre of the cross section, **b** CRIMSON casting at edge of the cross section, **c** gravity casting at the centre of the cross section and **d** gravity casting at the edge of the cross section

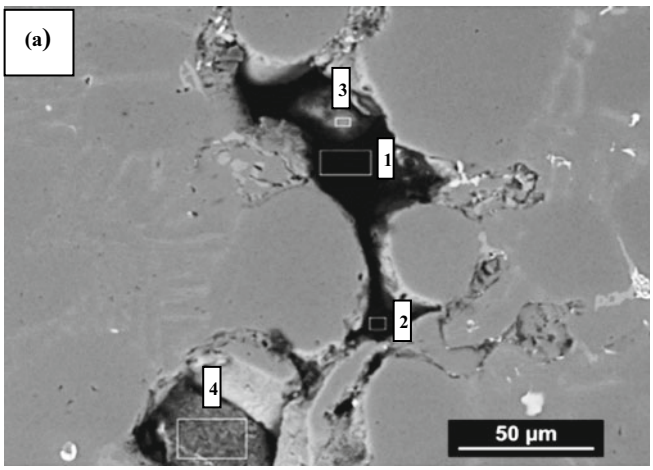

(b)

Element	1 (wt.%)	2 (wt.%)	3 (wt.%)	4 (wt.%)
O	14.02	12.56	5.41	12.34
Al	54.9	73.4	87.34	81.97
Si	7.99	1.61	1.64	3.15
Mn	-	-	-	0.52
Fe	-	-	-	0.85
Cu	23.09	12.44	5.6	1.17

Fig. 4 **a** SEM image of a DOF in the tensile gauge area gravity-cast microstructure. **b** EDS microanalysis of areas 1–4, as indicated in (**a**)

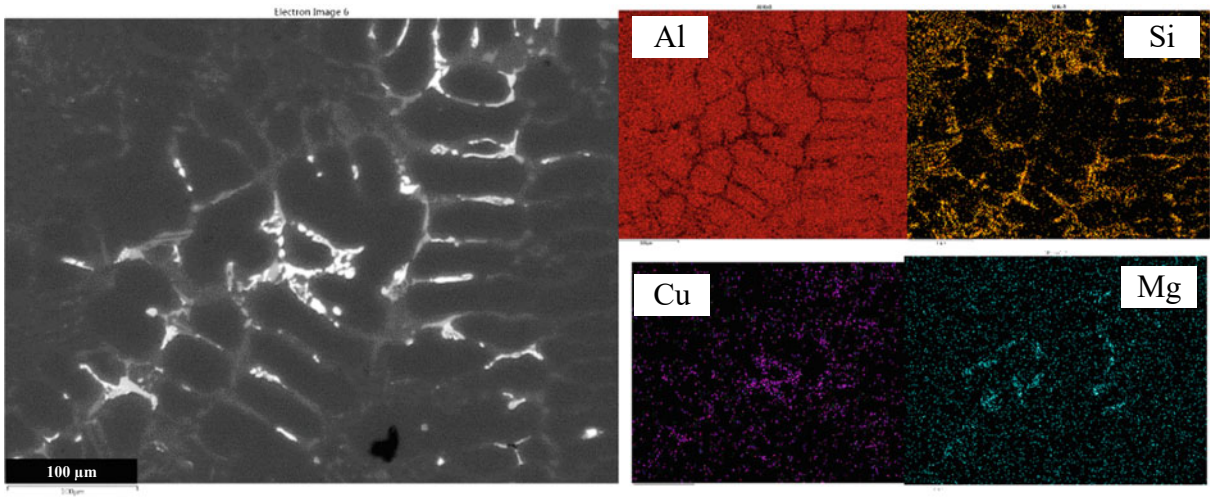

Fig. 5 Element mapping using SEM and EDS indicating the elemental distribution in secondary phases

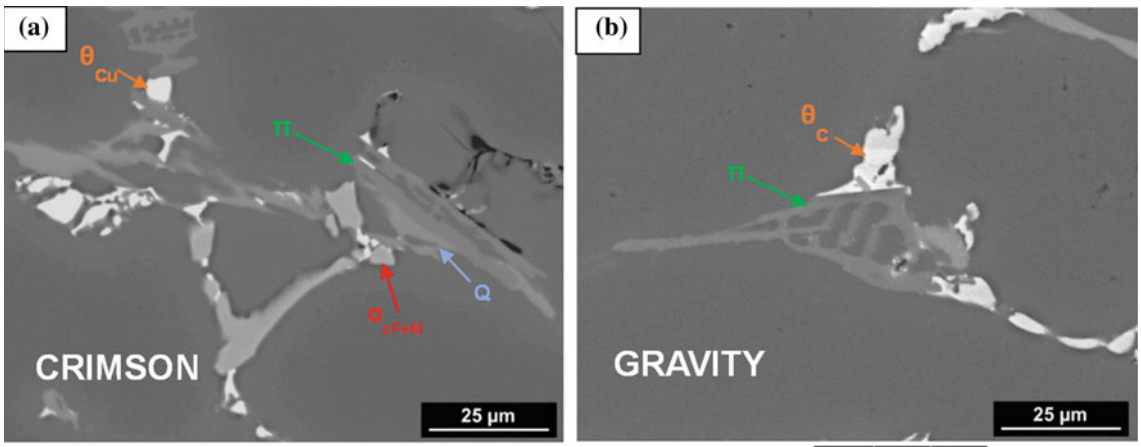

Element	α_{cFeMn} (wt.%)	Q (wt.%)	π (wt.%)	θ_{Cu} (wt.%)
Mg	-	23.07	13.54	1.63
Al	55.54	37	52.35	56.48
Si	9.74	22.35	23.37	2.35
V	0.39	-	-	-
Cr	0.27	-	-	-
Mn	15.97	-	2.21	-
Fe	11.6	0.37	7.57	-
Cu	6.49	17.2	0.94	39.54

Element	π (wt.%)	θ_{Cu} (wt.%)
Mg	12,18	-
Al	54,38	38,72
Si	22,07	-
Mn	0,81	-
Fe	7,38	0,52
Ni	0,94	8,58
Cu	2,22	52,18
Mg	12,18	-

Fig. 6 **a** SEM image of multiple intermetallic compounds clustered together as identified in CRIMSON castings. **b** SEM image of intermetallic compounds cluster found in gravity cast

both CRIMSON and gravity-cast samples revealing the presence of: (i) θ-Al_2Cu, (ii) Q–$Al_5Cu_2Mg_8Si_6$, (iii) π-$Al_8FeMg_3Si_6$, and (iv) α_cFeMn intermetallic compounds. The identification of the compounds was based on the chemical composition of the phases as well as their respective shapes [16]. The presence of the intermetallics, their morphology and size appear similar for both CRIMSON and gravity cast castings. As expected for aluminium–silicon–copper alloys the θ-Al_2Cu particles appear to form in spherical shapes, Q–$Al_5Cu_2Mg_8Si_6$ in irregularly rounded particles, π-$Al_8FeMg_3Si_6$ as Chinese script or branched polygons and α_cFeMn as branched polygons.

Hardness tests have shown an average value of 96.3 ± 11.2 HV and 88.0 ± 10.6 HV for the CRIMSON and gravity casting respectively. The standard deviation in both samples is at the anticipated range and it mainly derives from the hardness difference between the corresponding dendritic and eutectic areas. The yield strength (YS) and ultimate tensile strength (UTS) were found to be 151 MPa, 192 ± 22 MPa for CRIMSON sample, and 153 MPa,

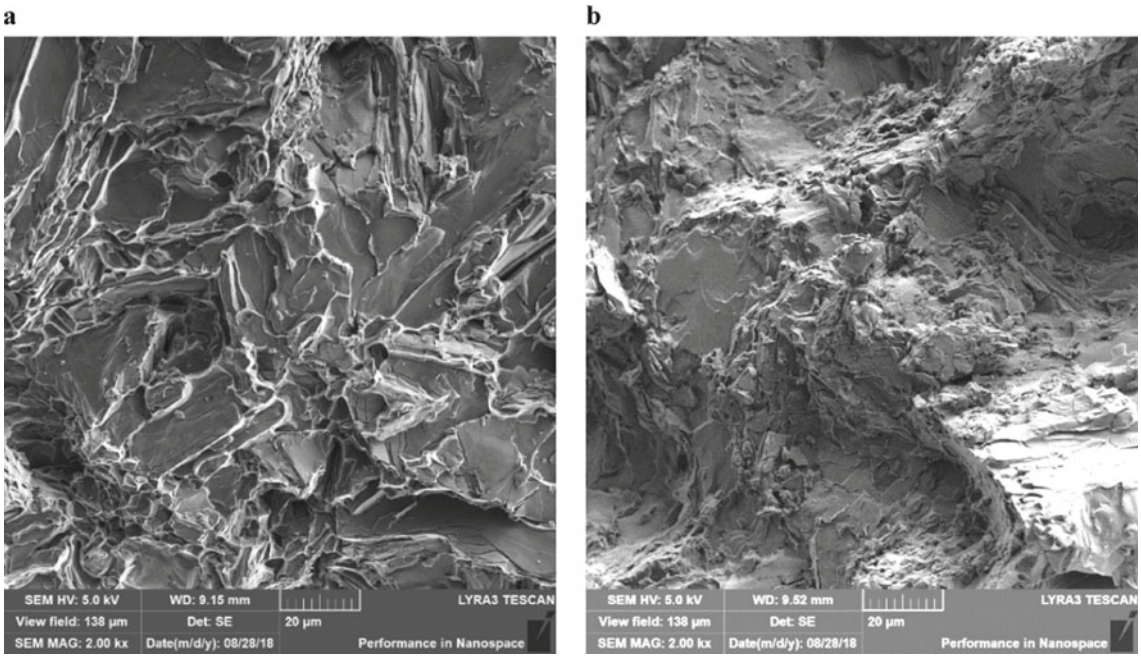

Fig. 7 Typical SEM images of the fractured surfaces after tensile tests: **a**, **b**, CRIMSON casting at low magnification, **c**, **d** gravity casting

195 ± 30 MPa, for gravity-cast samples, respectively, values comparable or better than expected for similar castings [17–19]. Plastic strain to failure was around 1% for CRIMSON and gravity castings. It is to be noted, that the mechanical strength and ductility usually improve with thermal treatment and ageing; this is the focus of an ongoing investigation. Figure 7 presents SEM images taken from typical fractured surfaces of the cast samples. Fracture analysis reveals a mixed fracture mode for the CRIMSON cast sample (Fig. 8a) with cleavage facets characteristics of (prevailing) brittle transgranular fracture coexisting with micro-dimples to a smaller extent. For the gravity-cast samples (Fig. 8b), the characteristics of brittle transgranular fracture are even more prominent and the evidence of ductile fracture much more scarce.

Amongst the important observations in this study, is the premature failure of a gravity-cast sample during tensile tests; the sample fractured without any plastic deformation at only a fraction of the expected UTS (~138 MPa). This premature failure was directly related to a sizable entrapped oxide defect, as shown in Fig. 7, covering about a third of the cross-sectional area. Whereas, such a sizeable defect was not detected in other gravity samples, this observation highlights the unreliability of conventional gravity casting processes and underlines the benefits from processes such as CRIMSON that can reliably produce castings with high structural integrity.

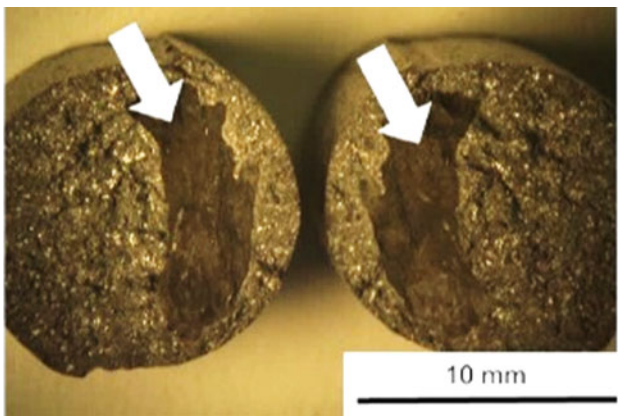

Fig. 8 The fractured surfaces from a gravity cast specimen fractured prematurely at a fracture of the UTS (~138 MPa) without any plastic deformation. The arrows indicate the entrapped oxide defect

Conclusions

In this work, the structure and mechanical properties of Al castings produced by CRIMSON counter-gravity casting method was investigated and compared with gravity-cast specimens. The 354 Al alloy was used in this case in the as-cast condition. The microstructure was investigated using XRD, OM, and SEM revealing similar findings for the two castings processes. The microstructure was investigated using XRD, OM, and SEM revealing similar findings for the two casting processes. Dendritic microstructure was revealed mainly consisting of α-Al dendrites and Al–Si eutectic, as expected in Al–Si hypoeutectic alloys. Furthermore, the presence of the following intermetallic compounds has been

confirmed: (i) θ-Al_2Cu, (ii) Q–$Al_5Cu_2Mg_8Si_6$, (iii) π-$Al_8FeMg_3Si_6$, and (iv) α_cFeMn. The mechanical properties were found to be similar for the CRIMSON and gravity cast A354 alloy in terms of tensile strength and hardness. This is believed to be relevant to the similarity in the microstructure of the alloys. Interestingly, significant differences were found between the CRIMSON counter-gravity and the conventional gravity castings in terms of porosity and oxide bifilms. Microscopical examination revealed a significant reduction in the presence of pores relevant to air entrainment as well as oxide inclusions and bifilms for the CRIMSON counter-gravity cast samples, mainly achieved due to the controlled liquid flow during filing; in contrast to the turbulent flow during the conventional filing in gravity casting. The elimination of large pores and oxide defects in CRIMSON castings has a major impact on the structural integrity and the expected fatigue resistance of the castings, improving in parallel the casting yield of the process.

Acknowledgements Financial support from the EPSRC-DTP project "Low Energy Casting: Novel Induction Technologies for Energy Efficient Rapid Melting" (ref 2,541,199) in the framework of (EP/R513027/1) and the UK EPSRC project "Energy Resilient Manufacturing 2: Small is Beautiful Phase 2 (SIB2)" is gratefully acknowledged.

References

1. Campbell J (2003) Castings. Elsevier, Oxford
2. Jolly MR (2003) Castings, in: Milne I, Ritchie RO, Karihaloo B (Eds.), Comprehensive Structural Integrity, 1st ed., Elsevier, Oxford, 2003, p 377–466.
3. Jolly M, Katgerman L (2022) Modelling of defects in aluminium cast products. Progress in Materials Science 123: 100824
4. Divandari M, Campbell J (2004) Oxide film characteristics of Al-7Si-Mg alloy in dynamic conditions in casting. International Journal of Cast Metals Research 17(3):182-187. https://doi.org/10.1179/136404604225017546
5. Ktari A, El Mansori M (2021) Intelligent approach based on FEM simulations and soft computing techniques for filling system design optimisation in sand casting processes. The International Journal of Advanced Manufacturing Technology 114(8):981-995. https://doi.org/10.1007/s00170-021-06876-z
6. Campbell J (2012) Stop Pouring, Start Casting. Intern. Journal of Metal Casting 6: 7–18. https://doi.org/10.1007/BF03355529
7. Archer L, Hardin RA, Beckerman C (2018) Counter gravity sand casting of steel with pressurization during solidification, Intern J. of Metal Casting, 12 (3): 596-606
8. Dai X, Jolly M, Zeng B (2012) The improvement of aluminium casting process control by application of the new CRIMSON process. IOP Conference Series: Materials Science and Engineering 33:012009. https://doi.org/10.1088/1757-899X/33/1/012009
9. Papanikolaou M, Pagone E, Georgarakis K, Rogers K, Jolly Mark, Salonitis K. (2018) Design Optimisation of the Feeding System of a Novel Counter-Gravity Casting Process Metals, 8(10): 817; https://doi.org/10.3390/met8100817
10. Li Y, Georgarakis K, Pang S, Antonowicz J, Charlot F, LeMoulec A, Zhang T, Yavari AR (2009) AlNiY chill-zone alloys with good mechanical properties, J. Alloy. Compd., 477: p 346-349
11. Li Y, Georgarakis K, Pang S, Antonowicz J, Charlot F, LeMoulec A, Zhang T, Brice-Profeta S., Zhang T, Yavari AR (2009) Chill-zone aluminum alloys with GPa strength and good plasticity, J. Mater. Res., 24: p 1513-1521
12. Wang Z, Qu RT, Scudino S, Sun BA, Prashanth KG, Louzguine-Luzgin DV, Chen MW, Zhang ZF, Eckert J (2015) Hybrid nanostructured aluminum alloy with super-high strength. NPG Asia Mater. 7: p. e229
13. Dong X, Yang H, Zhu X, Ji S (2019) High strength and ductility aluminium alloy processed by high pressure die casting, J. Alloys Compds, 773: p 86-96
14. Toschi S, (2018) Optimization of A354 Al-Si-Cu-Mg Alloy Heat Treatment: Effect on Microstructure, Hardness, and Tensile Properties of Peak Aged and Overaged Alloy. Metals 8: p 961 https://doi.org/10.3390/met8110961
15. Campbell FC (2013) Metals Fabrication; Understanding the Basics. ASM International, Materials Park, Ohio
16. Brown, JR (2000) Foseco Non-Ferrous Foundryman's Handbook. Butterworth-Heinemann, Oxford.
17. Shabestari SG, Moemeni H (2004) Effect of copper and solidification conditions on the microstructure and mechanical properties of Al-Si-Mg alloys. Journal of Materials Processing Technology 153–154:193–198. https://doi.org/10.1016/j.jmatprotec.2004.04.302
18. Tiryakioglu, M. (2020) The effect of hydrogen on pore formation in aluminum alloy castings: Myth versus reality. Metals 10(3) p 368; https://doi.org/10.3390/met10030368.
19. Campbell, J (2018) Mini Casting Handbook. Aspect Design, Malvern.